

Architectural Elements of Hybrid Navigation Systems for Future Space Transportation

Guilherme F. Trigo* Stephan Theil†

Abstract The fundamental limitations of inertial navigation, currently employed by most launchers, have raised interest for GNSS-aided solutions. Combination of inertial measurements and GNSS outputs allows inertial calibration on-line, solving the issue of inertial drift. However, many challenges and design options unfold. In this work we analyse several architectural elements and design aspects of a hybrid GNSS/INS navigation system conceived for space transportation. The most fundamental architectural features such as coupling depth, modularity between filter and inertial propagation, and open-/closed-loop nature of the configuration, are discussed in the light of the envisaged application. Importance of the inertial propagation algorithm and sensor class in the overall system are investigated, being the handling of sensor errors and uncertainties that arise with lower grade sensory also considered. In terms of GNSS outputs we consider receiver solutions (Position and Velocity) and raw measurements (Pseudorange, Pseudorange-rate and Time-Differenced Carrier Phase). Receiver clock error handling options and atmospheric error correction schemes for these measurements are analysed under flight conditions. System performance with different GNSS measurements is estimated through covariance analysis, being the differences between Loose and Tight coupling emphasised through partial outage simulation. Finally, we discuss options for filter algorithm robustness against non-linearities and system/measurement errors. A possible scheme for Fault Detection, Isolation and Recovery is also proposed.

1 Introduction

GNSS-aided navigation is slowly making its way into space transportation applications. Either as part of the vehicle's main navigation system or serving as on-board safeguard tracking measure, satellite-based positioning technology is increasingly found in launchers and sounding rockets. As opposed to inertial-only navigation, GNSS solutions have bounded errors. Therefore, if coupled with inertial measurements, GNSS position and velocity information bounds the overall solution, correcting for inertial biases and scale factors. Although this approach is common in land-based and aeronautical applications [21], most

*German Aerospace Center (DLR), Institute of Space Systems, GNC Systems Department
`guilherme.trigo@dlr.de`

†German Aerospace Center (DLR), Institute of Space Systems, GNC Systems Department
`stephan.theil@dlr.de`

launch vehicle navigation schemes are still purely inertial. Measurements from strapped-down accelerometers and gyroscopes are integrated yielding a high-rate solution which, despite robust, inevitably drifts over time [56]. Acceptable error growth is only achieved with highly accurate sensors which are generally very costly and heavy. Nevertheless, drift is still present, posing important mission performance and operational constraints. Injection accuracy, for instance, depends greatly on navigation solution quality and, thus, deteriorates with mission length [3]. Nominal mission trajectory and mission profile are also highly limited by inertial drift [11].

In a GNSS/INS (hybrid) navigation configuration, the strengths of both systems ease each others' flaws: the low-rate bounded GNSS information corrects the high-rate inertial propagation while the latter smoothly bridges satellite signal outages. In a launch environment, however, satellite navigation faces important vulnerabilities. As non-self-contained system, signal disturbances and disruptions can occur (e.g. jamming, spoofing, tropospheric and ionospheric effects). Additionally, the receiver tracking loops are not immune to the high-dynamics, vibration and shocks of launch flight [5]. These risks are reduced and their effects lessened by the combination of GNSS and inertial measurements.

The design of such a hybrid navigation system for space transportation applications faces a variety of challenges and design options which need to be addressed. In this contribution we investigate several of the key architectural elements involved in this design having in mind the target application.

This paper starts by presenting, in Section 2, a brief description of the current status of launcher navigation in terms of limitations posed by the purely-inertial methods and examples of existing GNSS-based systems. Some of the existing requirements for such systems are also shortly discussed. Section 3 discusses the most fundamental design options of GNSS/INS hybrid navigation systems intended for use in space transportation. The inertial navigation elements of the hybrid set-up are looked into in Section 4. There, the strapdown algorithm and propagation rate are tested on a sounding rocket trajectory, illustrating the influence of dynamical effects. Exemplary profiles of three inertial sensor classes are then tested both in dead-reckoning and in hybridized configurations. Means of handling the errors related to lower grade sensory are also shortly discussed. Section 5 looks into some of the GNSS outputs available. Their source and characteristics are presented and ways of handling their errors are introduced. Hybrid navigation performance obtained with different sets of these measurements is then estimated through covariance analysis. Finally, the filter core algorithm selection in the face of system non-linearities and robustness requirements is discussed in Section 6. Fault tolerance and means of detection and isolation in a hybrid navigation system are also briefly approached. A summary of conclusions closes the paper.

2 Launch vehicle navigation

Navigation information is fundamental to a launch mission. The navigation solution is used by the Guidance and Control system to guide and steer the vehicle, and may be sent via telemetry to ground control segment for monitoring. These two functions are commonly referred to, respectively, as navigation and safeguard. The Ariane-V, for instance, uses two identical and independent inertial units running in parallel: a *primary*, fulfilling the navigation function, and a *secondary*, used for both redundancy (replacing the primary in case of fault) and for safeguard. This section presents some of the limitations of inertial navigation when fulfilling these two tasks, and briefly lists several instances of GNSS-based developments aiming at overcoming them. Possible requirements and challenges faced by GNSS-Inertial hybrid systems developed for launch scenarios are also discussed.

2.1 Limitations of the inertial way

The dead-reckoning nature of inertial navigation yields continuous solution accuracy degradation. This imposes a series of strong limitations on launch missions. The following points describe some of the most important effects and constraints.

- Trajectory maintenance and payload injection accuracy are highly influenced by navigation error. This dependence can be as high as 90% [11]. Typical delivery dispersions are such that it is common that orbital correction manoeuvres need to be performed by the injected Spacecraft. These often have high Delta-V costs, potentially reducing mission life-time by months, years even, with considerable loss of commercial/scientific profit. Alternatively, fuel margins need to be taken into account from spacecraft development phase, sacrificing precious payload mass. In either case, several days may be required for an orbital correction planing and execution, potentially increasing LEOP (Launch Early Operation Phase) duration and cost.
- Mission duration and profile are strongly limited by the continuous degradation of navigation knowledge. Long and complex multi-phase missions often result in less accurate payload delivery or, to avoid this, need to include ground-based orbital determination phases, which are costly and lengthy. Return and landing phases of future reusable vehicle missions are simply not feasible with inertial-only navigation [44].
- The nominal trajectories in early ascent phases are defined to lie within visibility regions of ground tracking radars. These also include large margins that account for the drift in on-board navigation information, often representing a sacrifice of fuel optimality.

- If the inertial navigation solution is used for state monitoring and safeguard purposes, as it is done in Ariane-V in support to ground radar, the inertial drift translates into a growing state uncertainty ellipse. As the radar infrastructure used also has considerably limited accuracy, especially in velocity measurement, the result is a large uncertainty around the IIP (Immediate Impact Point) computed on-ground from all available data. The typical size of this region is used, pre-flight, to define an exclusion area at sea.

2.2 GNSS in launch vehicle navigation

GNSS technology is in many instances a remedy for the limitations imposed by inertial drift. Several launch navigation/tracking systems have been developed based on or including GNSS measurements.

One of the very first systems, the Space Integrated GPS/INS, or SIGI, designed by Honeywell under a NASA contract, has been extensively tested on-board of space transportation systems. These included the Space Shuttle, the X-37 and X-38 vehicles [26, 46, 62], and the International Space Station [16, 17]. This system was conceived to play the role of primary navigation system and is envisaged to figure as part of the GNC system of the Orion space vehicle [37]. Also in the U.S., GPS Metric Tracking systems (GPS MT), a class of on-board GPS-based tracking and telemetry systems, have been targeted as replacement technology for the C-band radar tracking, as part of the initiative for decommissioning of these facilities. Under this initiative, United Launch Alliance has developed a GPS MT localization system with L1 and L2 bands for its launchers using COTS components [7]. This system is routinely flown on Atlas V and Delta IV launchers as main tracking means [1, 9]. Another GPS-based safety tracking system for launchers, the Autonomous Flight Safety System (AFSS), was developed by NASA Goddard Space Flight Center and Wallops Flight Facility [13]. This COTS-based system follows a flexible vehicle, mission, and range-based approach, being configured and tuned prior to each flight according to the scenario. Since development Phase III of the project, it allows the inclusion of an IMU coupled with the GPS receiver. Other GPS MT systems for tracking of small launch vehicles and sounding rockets are currently under development [47, 61].

In Russia, a hybrid INS/GLONASS/GPS primary navigation system has been successfully used on-board of the Fregat upper stage launched by both Soyuz-2 and Zenit-SM vehicles. After several flights, the attained orbital injection accuracy improvement with respect to purely inertial navigation was up to 10 times in MEO delivery missions and 100 times in GTO/GEO ones [11].

More recently, the Chinese launcher Long March 7 (CZ-7) has been suited with a loosely coupled GNSS/INS system fulfilling the role of primary navigation [54].

In Europe the experience with GNSS receivers on-board of launch vehicles is still gaining momentum. Due to the lack of redundancy in the tracking of the VEGA launcher, a COTS GPS receiver is currently flown as part of the

ALTS (Autonomous Localization and Telemetry Subsystem). This is planned to be coupled with a COTS inertial sensor in future flights [14]. In Ariane-V, as part of the OCAM-G payload, a set of three commercial GNSS receivers flew on-board of this European launcher [23]. This initiative was purely experimental and realized as a cooperation between ESA and European national space agencies and industry partners. However, there is strong evidence of will to consider GNSS-based tracking and navigation in the development of a future generation European launcher [34]. In what comes to the use of GNSS in primary navigation, an extensive study funded by ESA was carried out by Airbus SD and culminated in the development of HiNAV (Hybrid Navigation System). This project aimed at creating a prototype coupled GNSS/INS navigation system for European launch and re-entry vehicles and revealed promising results [41]. DLR has also developed and successfully flown a hybrid GPS/INS system on its SHEFEX-2 experimental flight, the HNS. This was conceived to work as primary navigation block employing a COTS IMU, a GPS receiver and a star sensor [51, 53, 55]. In addition to this, DLR has gathered important experience in the development and flight-test of GPS receiver technology for rocket applications with the Orion receiver [33] and more recently the Phoenix-HD receiver [30].

2.3 Challenges and requirements for Hybrid Navigation

The possible requirements and design challenges for a hybrid navigation system applied to space transportation can form a vast list. These may not only depend on the vehicle carrying it but also on whether the system is to act as primary navigation, as safeguard localization and tracking, or as both (serving as safeguard and switching to main navigation in case of failure of the primary system). Being a relatively new technology in the space transportation field, regulation and requirement documentation does not abound. Nevertheless, the following guidelines form a natural starting point:

- a GNSS-based on-board safeguard tracking system should at the very least match the accuracy level of the means currently used for vehicle tracking (e.g. radar stations);
- a GNSS-aided primary navigation system should achieve a worst case performance equivalent to that of the purely-inertial navigation systems now in use.

In the design process of an inertially-aided GNSS receiver for launcher tracking, Braun et al. [5] work out a set of performance requirements departing from: the accuracy of the currently used C-band tracking radars at Kourou Space Center; and from the U.S. range safety standard general performance requirements for GNSS receivers used as on-board tracking devices [15]. The authors arrive at a figure for the maximum tolerable instantaneous velocity error norm (~ 8.7 m/s).

Example of a more extensive set of design and functional requirements for a GNSS-based navigation system to be used both as safeguard and as primary navigation on Ariane-V can be found in [3]. The set includes architectural re-

quirements such as functional separation between GNSS receiver, inertial measurement unit, and navigation fusion computer. The authors state as preferable to forgo dynamic state aiding to the receiver as to maintain a fail-operational set-up. Further listed requirements target not only output accuracy (25 m and 0.25 m/s $1\text{-}\sigma$) but also robustness (e.g. against signal interference) and general reliability. A maximum failure rate level of 10^{-4} per hour during ascent and LEO phases is stated and GNSS failure detection and isolation is required.

These requirements represent a great challenge to the design of a Hybrid Navigation system. Vibration and shocks during engine burns and separation events not only perturb the inertial measurements but can also disrupt the tracking loops of the GNSS receiver causing signal loss and measurement drop-out. Signal loss can also be caused by ionospheric scintillations, while changing tropospheric delays during lower ascent disturb the receiver velocity measurement [57]. Finally, attitude observability is rather limited in a launch trajectory, particularly around roll axis, and especially in spinning rockets, creating a strong constraint on the selected gyroscope class.

3 Hybrid Navigation basic architecture

Combination of inertial and GNSS measurements is by no means new. It is, in fact, a matter of research since the early days of GPS [27]. Since then, various architectures have been proposed and implemented for several applications with different required performances. This section discusses some of the fundamental architectural options the light of space transportation.

3.1 Coupling Depth

One of the most basic architectural features of a hybrid navigation system is the depth of coupling between inertial sensor and GNSS receiver. Fig. 1 depicts three levels: loose, tight and ultra-tight.

The simplest of the presented set-ups is the *loosely* coupled system (Fig. 1a). This uses the GNSS receiver navigation solution to correct the inertial propagation through a fusion algorithm (e.g. a Kalman filter) [19]. The *tightly* coupled hybridization (Fig. 1b) uses directly the raw GNSS measurements (e.g. Pseudorange, Pseudorange-rate, Carrier Phase, etc.), avoiding the solution step within the receiver [27]. In these two configurations the fused estimates can be provided as aiding to the GNSS receiver to expedite satellite (re)acquisition. Finally, a closer coupling, usually called *ultra-tight* or *deep*, can be achieved by using the corrected inertial estimates to drive the receiver code and carrier tracking loops (Fig. 1c). In this set-up the navigation computer receives the accumulated correlator outputs (**I** and **Q**) from the receiver, fusing them directly with inertial measurements [21].

In general, the tighter the coupling the more complex the system becomes, but also the better the performance and, especially, robustness it delivers [21]. For instance, using a GNSS solution (instead of raw measurements) prevents

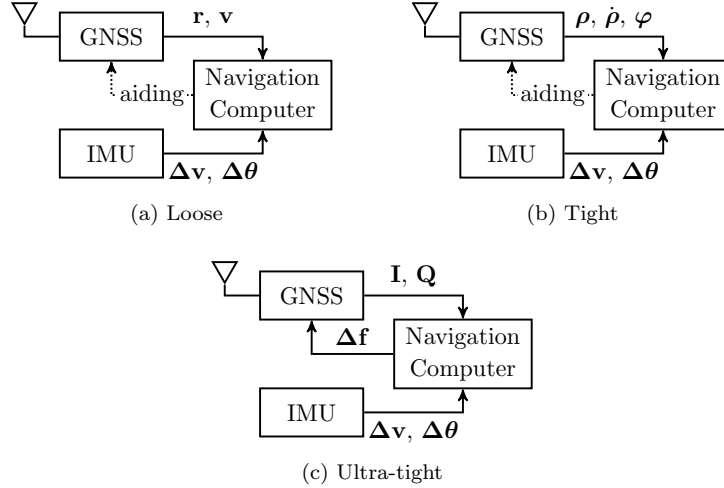


Figure 1: GNSS/Inertial coupling architectures.

the navigation from drawing information from sets of fewer than four tracked satellites [38]. This is limiting, for example, if an outage occurs and signals are gradually reacquired, or if the outage is partial and fewer than four signals are still tracked, as it is likely to happen during high dynamic phases of launch. A less obvious disadvantage of a loosely coupled scheme is the cascade of navigation filters; by having a first filter stage at the receiver (for GNSS navigation solution) the input to the navigation computer has noise components which are heavily time-correlated with variable profile. This may cause severe mismodelling, potentially degrading performance and robustness, and, in the extreme case, lead to instability [27]. Receiver requirements for loose and tight integrations do not dramatically differ, as off-the-shelf receivers usually output raw measurements together with the navigation fix. The ultra-tight hybridization, having a close link between receiver tracking loops and inertial propagation and correction, can achieve the very best results. It can withstand considerably lower C/N_0 conditions and operate under higher dynamics. However, its design requires either extensive access to the internal functioning of the receiver or parallel development of both receiver and hybrid system sides. The design and development complexity of such a system is thus far greater than the lower coupled options. Moreover, in this set-up a fail-operational architecture may not be achievable given the inter-dependence of GNSS tracking loops and inertial data. The two less coupled configurations offer, more or less readily, the possibility to isolate GNSS and Inertial platform functions, being thus preferable for the application at hand. For the reasons just stated, the ultra-tight architecture will not be pursued further in the study herein.

As an additional note on coupling, it is worth mentioning that an *uncoupled* architecture is also possible. An example is the system described by Belin et al.

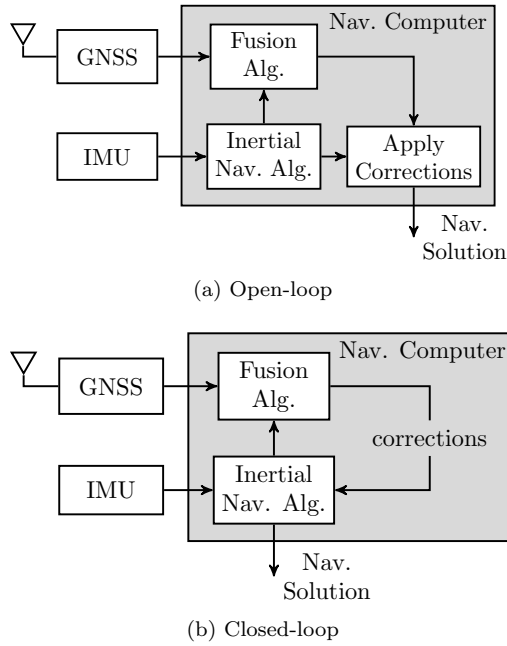


Figure 2: Open- and closed-loop configurations of a GNSS/Inertial system.

[3] for the tracking of Ariane-V, which parallelly runs an inertial platform and a GNSS receiver (with no connection between them). The solution of both devices is sent to ground for safeguard and state monitoring.

3.2 Open- vs Closed-loop

Another architectural option has to do with the open-/closed-loop nature of the estimated navigation corrections [21]. Fig. 2 shows the difference between open- and closed-loop hybridizations. In the open-loop configuration (Fig. 2a) the fusion algorithm estimates corrections to be applied to the inertial propagator output (position, velocity and attitude). These corrections may grow indefinitely as the inertial solution drifts. Instead, the inertial propagation may be regularly reset using the fused estimates in a closed-loop set-up (Fig. 2b). This makes sure that the filter remains close to the origin, reducing linearization errors and numerical issues due to unbounded state growth. Moreover, it allows for the inertial sensor online calibration, which offers higher robustness and greatly improves performance during outage. Both of these features are fundamental for the studied application. Note that, for the fulfilment of a fail-operational requirement, a second uncorrected inertial propagation may be carried out parallelly (within the inertial unit or in a separate computer).

3.3 Modularity and Direct/Indirect Filtering

Within the closed-loop configuration the degree of modularity between integration filter and inertial propagation algorithm is yet another design option. If the two are independently defined, having the filter estimate error quantities, the set-up is said to follow an *indirect* filtering scheme (and a modular integration). Shall the filter estimate, instead, total kinematics quantities and the inertial propagation be done as part of the state propagation of the filter the set-up is known as *direct* filtering (non-modular). Although architecturally distinct the performances of these two set-ups can be made virtually equivalent [21]. Potential differences in behaviour may however arise from the way the corrections are done [59]. The direct filtering scheme is, in general, more computationally intensive [59] and offers less design flexibility. Furthermore, as Steffes [50] shows, the indirect filtering architecture provides a simple yet powerful way to deal with measurement latency in the real-time implementation. This is a crucial feature as the outputs (both raw and processed) of most GNSS receivers carry considerable delays. Latencies of up to 500 ms are common [48]. In a launch scenario these simply cannot be neglected.

4 Inertial navigation elements

Inertial navigation is the process by which measurements given out by accelerometers and gyroscopes are used to track the vehicle's position and attitude with respect to a known starting condition. We focus on strapped-down platforms, as stable (gimballed) ones have become far less common in the field of launcher navigation. The absence of gimbals or frames makes strapdown mechanically simpler, smaller and lighter; however, considerably more complex algorithms are required to integrate the inertial measurements. This section briefly discusses this integration process, typical figures of different sensor quality classes and ways to account for their errors. The achievable Hybrid Navigation performance for different sensor grades is estimated by covariance analysis.

4.1 Strapdown integration

Fig. 3 presents a diagram of the propagation of inertial measurements used to generate a navigation solution. This process can be done either by the on-board (avionics) computer or by the measurement unit itself, which in such case it is referred to as Inertial Navigation System (INS) or Platform.

Samples of angular velocity and acceleration ($\boldsymbol{\omega}^B$, \mathbf{a}^B) or, more commonly, angular and velocity increments ($\Delta\boldsymbol{\theta}^B$, $\Delta\mathbf{v}^B$) are measured by the IMU in a body-fixed frame (here denoted B) and, generally, output at a constant rate.

The kinematic states propagation from t_j to t_{j+1} can be written in an inertial

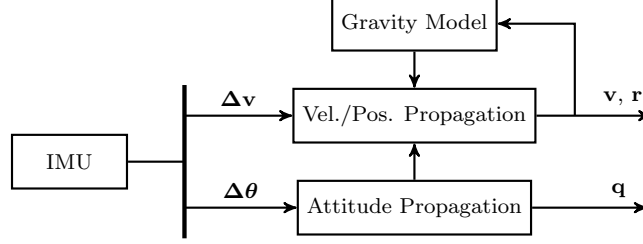


Figure 3: Strapdown inertial propagation process.

frame I as

$$\mathbf{C}_{B_{j+1}}^I = \mathbf{C}_{B_j}^I \exp \left(\int_{t_j}^{t_{j+1}} [\boldsymbol{\omega}^B \times] dt \right) = \mathbf{C}_{B_j}^I \Delta \mathbf{C}_{B_{j+1}}^{B_j} \quad (1a)$$

$$\mathbf{v}_{j+1}^I = \mathbf{v}_j^I + \int_{t_j}^{t_{j+1}} \dot{\mathbf{v}}^I dt = \mathbf{v}_j^I + \Delta \mathbf{v}_{\text{sf},j+1}^I + \Delta \mathbf{v}_{\text{g},j+1}^I \quad (1b)$$

$$\mathbf{r}_{j+1}^I = \mathbf{r}_j^I + \int_{t_j}^{t_{j+1}} \mathbf{v}^I dt = \mathbf{r}_j^I + \Delta \mathbf{r}_{j+1}^I, \quad (1c)$$

where $\Delta \mathbf{v}_{\text{g},j+1}^I$ is the gravitational correction and $\Delta \mathbf{C}_{B_{j+1}}^{B_j}$, $\Delta \mathbf{v}_{\text{sf},j+1}^I$ ¹, and $\Delta \mathbf{r}_j^I$ are the motion integrals computed from the inertial increments measured. Note that, as depicted in Fig. 3, the propagated attitude (and its increments) are used also by the linear motion integration, making it a crucial element in the strapdown method.

4.1.1 Reference frame considerations

While the navigation system mechanisation is easiest expressed in an Inertial reference frame as written in (1), there may be advantages to propagating the strapdown solution in a different frame. GNSS outputs are generally expressed in an Earth-Centred Earth-Fixed (ECEF in short, see [56] for a definition), thus it is common for GNSS/INS applications to integrate the kinematics solution with respect to this frame. The rotating nature of ECEF introduces a Coriolis term and frame rotation transformations which slightly complicate the mechanisation [56]. However, simplifications in the GNSS measurement update models of the fusion algorithm are obtained. Although far more used in aeronautical applications, a Local Geographic reference frame, such as NED (North-East-Down) or ENU (East-North-Up), can also be used. In this case, the mechanisation equations complicate further as an additional frame rotation motion needs to be considered, accounting for the change in the local surface tangent caused by the vehicle translation [56]. In on-board tracking systems intended to operate only during the first few minutes of flight it may make sense

¹The underscript *sf* stands for Specific Force, i.e. acceleration of non-gravitational origin.

to use a launch-pad/radar-station fixed frame for the mechanisation. Tracked states could then be azimuth, slant-range (or downrange), and elevation (or altitude). Such configuration may be especially suited for sounding-rocket-like applications that cover very short downrange distances.

4.1.2 Integration rate and dynamic effects

Numerous algorithms have been derived to solve the motion integrals in equations (1) [25, 31, 42, 43]. The two greatest concerns behind the development and selection of such methods are computational efficiency, and robustness against dynamics effects. While the former has an obvious origin: the on-board computing power is a limited resource; the latter is considerably more complex to grasp and tackle.

The rotation integral in (1a) can be exactly computed from non-infinitesimal angular increments if the angular velocity direction is constant within the integration period. In an unconstrained vehicle, however, this is generally not the case. The simplest approximation then is to assume that the sampling period (between t_j and t_{j+1}) is small enough so that the changes in rate direction are negligible, i.e.

$$\begin{aligned} \int_{t_j}^{t_{j+1}} \boldsymbol{\omega}^B dt &\approx \Delta\boldsymbol{\theta}_{j+1}^{B_{j+1}} \\ \int_{t_j}^{t_{j+1}} \dot{\mathbf{v}}^I dt &\approx \mathbf{C}_{B_{j+1}}^I \Delta\mathbf{v}_{j+1}^{B_{j+1}} + \Delta\mathbf{v}_{\mathbf{g},j+1}^I, \end{aligned} \quad (2)$$

where $\Delta\boldsymbol{\theta}_{j+1}^{B_{j+1}}$ and $\Delta\mathbf{v}_{j+1}^{B_{j+1}}$ are the gyroscope and accelerometer incremental measurements for such interval. The attitude, velocity and position propagation equations (1a)-(1c) can then be solved. This corresponds to a first order, full-rate propagation. Higher order solutions of the integrals in (2) are possible [31, 57].

Decreasing the computational cost of this process is possible by widening the integration interval of (2), simply summing up inertial increments in batches as

$$\begin{aligned} \int_{t_j}^{t_{j+N}} \boldsymbol{\omega}^B dt &\approx \sum_{k=1}^N \Delta\boldsymbol{\theta}_{j+k}^{B_{j+k}} \\ \int_{t_j}^{t_{j+N}} \dot{\mathbf{v}}^I dt &\approx \mathbf{C}_{B_{j+N}}^I \sum_{k=1}^N \Delta\mathbf{v}_{j+k}^{B_{j+k}} + \Delta\mathbf{v}_{\mathbf{g},j+N}^I, \end{aligned} \quad (3)$$

and using these to solve (1a)-(1c) at a lower rate with respect to the IMU output rate. This downsampling, however, can lead to severe inaccuracies as the validity of the ‘‘constant angular rate direction’’ assumption weakens. A classical example of an especially malign motion in such case is *coning*, which occurs when the angular velocity vector is itself rotating (describing a cone). A similarly malign motion, known as *sculling*, affects velocity and position integration [56]. Coning motion is rather common in spinning rockets. Moreover, high-frequency vibrations, as those experienced in launch, can also cause similar effects. While

in a Hybridized scheme sculling is well mitigated by the direct measurement of position and velocity by the GNSS receiver, coning poses a higher threat as attitude is not directly observed. The simplest way to prevent such effects is to perform the integration at the highest possible rate, i.e. at the output rate of the IMU. More efficient ways perform the integration at a lower rate, but apply better (and more complex) approximations than the simple summation in (3). These are commonly known as coning- and sculling-compensation algorithms, and can be high-rate iterative algorithms, as in [42, 43], allowing any rate-reduction ratio, or predefined laws optimized for a given number of subsamples [25]. Naturally, the inertial sensor output rate must be such that (at least) at full-rate integration the dynamic effects are tolerable.

Fig. 4 compares the strapdown propagation error (with respect to the full-rate integration at 400 Hz) for different levels of integration rate reduction with and without dynamical compensation. The compensation methods used for the 2, 3, 4 and 5 fold rate reductions are, respectively, Algorithms 2, 6, 8 and 10 in [25]. The trajectory followed is that of SHEFEX2 sounding rocket [51] and the inertial increments used in the integration are error-free; i.e. the errors plotted arise solely from dynamics effects on the propagation. Rate reduction leads to a clear increase of integration error; and while compensation algorithms ease this effect, especially for position and velocity, attitude accuracy loss quickly becomes significant. Mild reduction of inertial integration rate (2-3 times) in such a highly dynamic application is possible, but should be carefully traded-off against the effects of vehicle dynamics and trajectory. It should be noted that in a hybrid navigation system this accuracy loss will have the most impact on longer dead-reckoning periods, i.e. GNSS outages.

4.2 Inertial sensor class

Inertial units are commonly arranged in quality grades, ranging from Consumer- to Inertial/Strategic-grade [2, 56]. The strapdown gyroscope units used in launcher applications are generally based on optical technology: FOG (Fibre-Optic-Gyro) and RLG (Ring-Laser-Gyro). European launchers Ariane-V and Vega, for instance, carry Navigation-grade RLG-based units [5]. In sounding rockets and smaller launchers relatively lower grade units are used. For example, the SHEFEX2 sounding rocket employed a Tactical-grade FOG-based IMU [51]. In recent years, great effort has been put into the development and improvement of Micro Electro-Mechanical Systems (MEMS) for space applications [12, 18]. This class of devices spans from Consumer- to Tactical-grade sensors, all of which substantially lighter, smaller and cheaper than regular optical-based devices.

Table 1 displays exemplary specifications for Navigation- and Tactical-grade inertial sensors. The Navigation-grade gyroscope profile follows that of an RLG, while the Tactical-grade units considered are of the FOG and MEMS types.

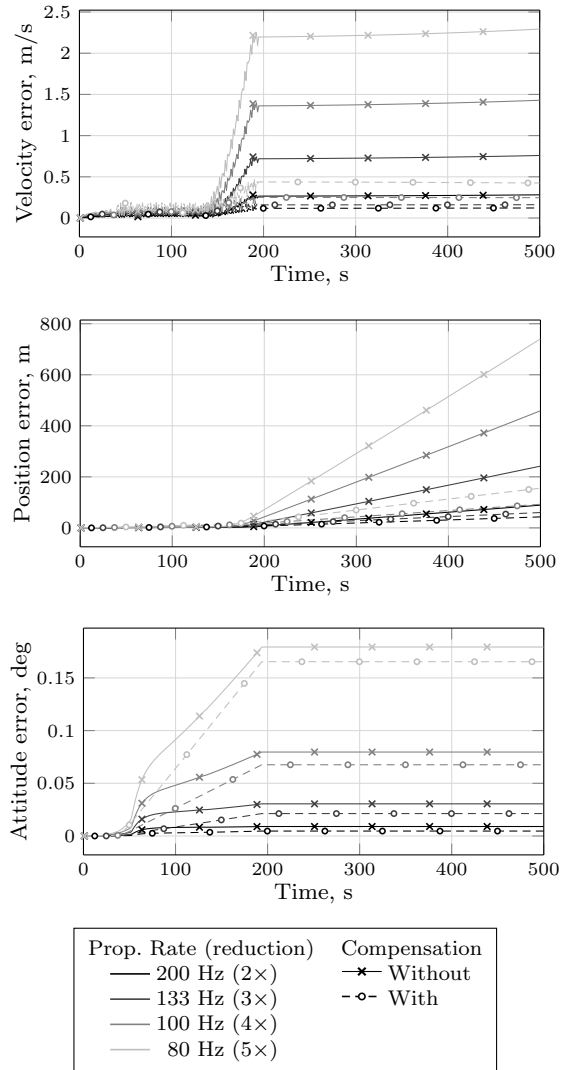


Figure 4: Propagation errors with respect to a full-rate integration (400 Hz), of several rate reductions (2, 3, 4 and 5 times) with and without dynamic compensation. Error-free inertial measurements of a SHEFEX2 trajectory (lift-off at 0s).

Table 1: Error specifications (1σ) for the three IMU grades considered.

Perturbation	Unit	Sensor Grade		
		Navigation	Tactical-FOG	Tactical-MEMS
Gyroscope				
Bandwidth	Hz	500	500	200
Axis Misalignment	mrad	0.1	0.5	1
Angle Random Walk	deg/ \sqrt{h}	0.005	0.03	0.2
Rate Random Walk	deg/h ^{3/2}	0.005	0.1	1
Bias Repeatability	deg/h	0.01	1	10
Bias Instability	deg/h	0.005	0.03	3
G-sensitive Bias	deg/h/g	0.01	0.01	10
Scale Factor Repeatability	ppm	10	300	1000
Scale Factor Drift (RW)	ppm/ $\sqrt{\text{year}}$	35	350	3500
Scale Factor Non-linearity	ppm FS	20	25	50
Accelerometer				
Bandwidth	Hz	500	200	200
Axis Misalignment	mrad	0.3	0.5	1
Velocity Random Walk	mg/ $\sqrt{\text{Hz}}$	0.1	0.05	0.5
Acceleration Random Walk	mg/ \sqrt{h}	0.05	0.5	2
Bias Repeatability	mg	0.1	2	3
Bias Instability	mg	0.01	0.05	0.05
Scale Factor Repeatability	ppm	30	1500	1500
Scale Factor Drift (RW)	ppm/ $\sqrt{\text{year}}$	1000	2000	2000
Scale Factor Non-linearity	ppm FS	150	300	300

4.2.1 Errors and error modelling

As illustrated by the specifications on Table 1, the perturbations affecting lower grade units are generally stronger. Some, as bias and scale-factor, also have faster rates of change. While in a purely-inertial set-up bias and scale-factor stability is absolutely crucial in ensuring the initial (on-ground) calibration remains valid as long as possible during flight, in a Hybrid scheme such requirement may be relaxed given the continuous calibration provided by the GNSS. However, if lower grade sensory is to be used, additional effort must be put into the modelling of inertial measurement perturbations within the fusion algorithm, or robustness and filter coherence may be at risk.

Stochastic errors of medium and lower class sensors tend to display time-correlations and to include strong bias instability levels (flicker noise). Allan variance analysis can be used to map and model these stochastic features through the fitting of Gauss-Markov processes [24]. Alternatively, classical Auto-Regressive (AR) modelling directly produces the process shaping filter coefficients [35]. Note that, the longer the operation time (i.e. the launch mission), the closer the modelling needs to fit the medium and long term features of the noise profile.

Turn-on scale-factor and scale-factor drift are considerably higher in lower

grade sensors. While a simple random-constant plus random walk model can be used to account for the constant and time-dependent components, the operation region dependency (known as non-linearity) is much more difficult to tackle. On-ground characterization can be used to mitigate the deterministic (and static) part of the scale-factor curve, however, the residual non-linearity may still result in significant error. Steffes [52] inflates the random walk values of the filter scale-factor model to render it robust to the non-linearity residual in a sounding rocket flight. Another possibility is to do this additional “injection” of uncertainty not continuously, but as a function of the change of operation region. In either case, these *ad-hoc* solutions should be carefully tuned according to the sensor and trajectory.

Due to the less strict manufacturing tolerances, the mutual alignment of sensing axes (also known as non-orthogonality) and the alignment of the triad to the sensor casing also tend to carry higher uncertainties with decreasing sensor grade. Consequently, as a complement to pre-flight alignment, residual misalignments (which also include those of the final assembly in the launch vehicle) should be accounted for in the fusion algorithm.

Depending on the design and working principle, gyroscopes can have g-sensitive bias components [56]. Whereas in units based on optical technology this dependence is usually negligible, MEMS units, based on mechanical principles, are particularly sensitive. Given the strong accelerations of launch, this is certainly one of the most important criteria in gyroscope selection. Modelling of this error within the fusion filter is possible and advisable if the sensor shows such sensitiveness.

4.2.2 Sensor class and navigation performance

As previously mentioned, the performance of purely-inertial navigation depends greatly on the quality of the inertial sensors employed. An example is given in Fig. 5, which shows the inertial propagation error covariances (velocity, position and attitude) for the three IMU profiles on Table 1 under a Vega launch trajectory. Considering the achieved error levels it becomes obvious the need for very accurate inertial sensors in such purely-inertial schemes.

Fig. 6, in turn, shows the expected error covariance levels if the same inertial information is fused with position and velocity fixes. The error covariance of the aiding position and velocity information was scheduled with altitude to coarsely emulate the effect of GNSS atmospheric errors (cf. Section 5.2). While position estimation accuracy is identical with all three sensor classes, depending entirely on the aiding quality, velocity and attitude show variation with the inertial sensor grade. This dependence is particularly high for the attitude, as this is not directly measured; nonetheless, fusion renders it partially observable, considerably improving its estimation with respect to the pure inertial integration. As a result, the attitude covariance levels of the aided configurations in this analysis show roughly a one-grade improvement over the dead-reckoning ones: the aided Tactical-FOG configuration approaches the level of the unaided Navigation grade sensor, whereas the aided Tactical-MEMS achieves an atti-

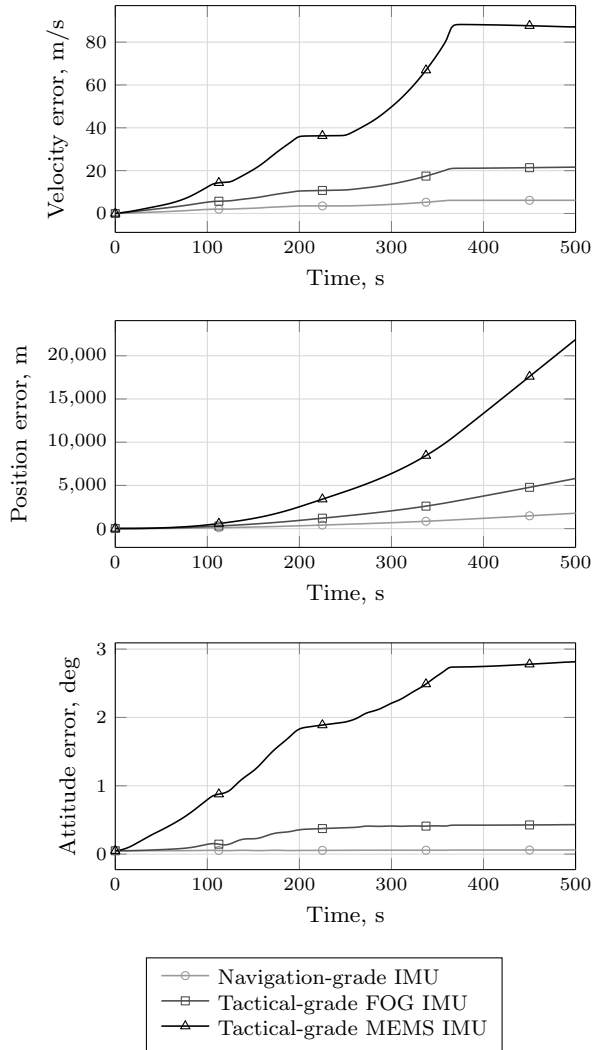


Figure 5: Error covariance ($1\text{-}\sigma$) of the propagation of inertial measurements from the IMU profiles on Table 1. Vega launch trajectory with lift-off at 0s.

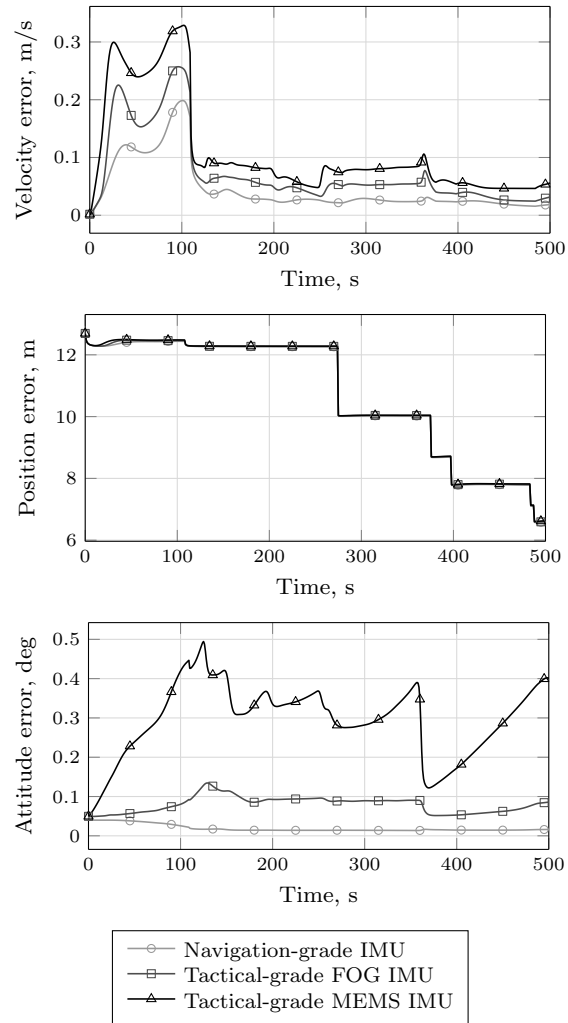


Figure 6: Error covariance ($1-\sigma$) of the fusion of inertial data from the IMU units on Table 1 and Position and Velocity fixes of GNSS-like quality. Vega launch trajectory with lift-off at 0 s.

tude accuracy level similar to the unaided Tactical-FOG sensor. This direct comparison is shown in Fig. 7.

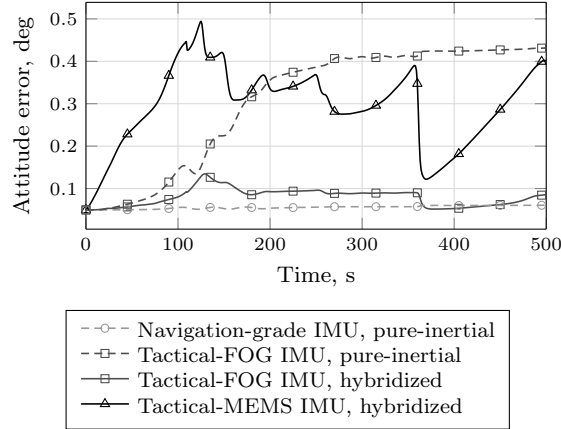


Figure 7: Comparison of attitude error covariance ($1\text{-}\sigma$) of pure-inertial and aided solutions from Fig. 5 and 6, respectively.

5 GNSS signals and models

In the design of loosely and tightly coupled Hybrid Navigation the selection of the GNSS measurements to be used is fundamental. Not only does it set the coupling depth (in the choice between processed and raw measurements), but also the achievable performance and robustness, by using or not velocity-based measurements as support to the more common position-based ones. Further flexibility lies in the modelling of the selected measurements. This section discusses several of the common GNSS outputs and possible models for the errors that affect them in the studied application. Hybrid Navigation performance in a launch scenario for different measurement sets is also looked into.

5.1 GNSS receiver outputs

A GNSS receiver may have several outputs. The most commonly used are the PVT (Position, Velocity, Time) solutions, which are derived from a set of *raw* measurements produced by the receiver's ranging processor. These are generally code and phase (or frequency) observables from each tracked satellite.

5.1.1 Pseudorange and Pseudorange-rate

Pseudoranges are generated from the time-of-flight measurements obtained by the receiver ranging processor (code tracking loop). Parallely, Pseudorange-rates are derived from the Doppler shifts measured by the carrier wave tracking

loop. These measurements can be given in terms of the real range and range-rate, ρ_i and $\dot{\rho}_i$, between receiver and satellite i at epoch k as

$$\tilde{\rho}_{i,k} = \rho_{i,k} + \rho_{e,i,k} + \nu_{\rho,i,k} \quad (4)$$

$$\tilde{\dot{\rho}}_{i,k} = \dot{\rho}_{i,k} + \dot{\rho}_{e,i,k} + \nu_{\dot{\rho},i,k}, \quad (5)$$

where $\rho_{e,i,k}$ and $\dot{\rho}_{e,i,k}$ are the range and range-rate errors, which may be induced, for instance, by receiver and satellite clock, atmospheric and multipath effects. $\nu_{\rho,i,k}$ and $\nu_{\dot{\rho},i,k}$ are receiver channel noises. Some of the errors affecting these measurements are discussed in Section 5.2.

Pseudorange is a position-based measurement, while pseudorange-rate is velocity-based. To keep the navigation system complexity low, it is not uncommon to use only Pseudoranges as update to the fusion algorithm. Indeed, the SHEFEX2 HNS used only this GNSS observable [52]. However, in highly dynamic applications such as launchers or sounding rockets, it may be beneficial to further include a measure of velocity. Braun et al. [5] fuse both Pseudorange and Pseudorange-rate with inertial measurements in a navigation system meant for launcher localization.

The model for range depends on vehicle and satellite antenna positions as

$$\rho_{i,k} = \left\| \mathbf{C}_{E(t_{s,i,k})}^{E_k} \mathbf{r}_{s,i}^E(t_{s,i,k}) - \mathbf{r}_{\text{ant},k}^E \right\|, \quad (6)$$

where the satellite position $\mathbf{r}_{s,i}^E$ is evaluated at the time of emission $t_{s,i,k}$ and translated to the ECEF frame at the time of reception. The position receiver antenna $\mathbf{r}_{\text{ant},k}^E$ is taken at the reception instant. The range-rate can be easily derived, accounting for the derivative of the signal travel time, as

$$\begin{aligned} \dot{\rho}_{i,k} &= \frac{d\rho_{i,k}}{dt} \\ &= \frac{\mathbf{e}_{\rho,i,k}^E \top \left(\mathbf{C}_{E(t_{s,i,k})}^{E_k} \left(\mathbf{v}_{s,i}^E(t_{s,i,k}) + \boldsymbol{\Omega}_{IE}^E \mathbf{r}_{s,i}^E(t_{s,i,k}) \right) - \mathbf{v}_{\text{ant},k}^E - \boldsymbol{\Omega}_{IE}^E \mathbf{r}_{\text{ant},k}^E \right)}{1 + \frac{1}{c} \mathbf{e}_{\rho,i,k}^E \top \mathbf{C}_{E(t_{s,i,k})}^{E_k} \left(\mathbf{v}_{s,i}^E(t_{s,i,k}) + \boldsymbol{\Omega}_{IE}^E \mathbf{r}_{s,i}^E(t_{s,i,k}) \right)}, \end{aligned} \quad (7)$$

where $\mathbf{e}_{\rho,i,k}^E$ is the unit range vector from receiver to satellite i , $\mathbf{v}_{s,i}^E$ is the satellite velocity, $\boldsymbol{\Omega}_{IE}^E$ is the skew-symmetric (cross-product) matrix of the Earth rotation vector written in ECEF coordinates, and c is the speed of light in vacuum.

5.1.2 Integrated Carrier Phase

The integrated carrier phase quantity is obtained by the receiver through the accumulation of the phase increments from the carrier tracking loop. This quantity is directly proportional to the range increment (Delta) since the beginning of the integration. It is the GNSS (raw) observable with the lowest noise level [22]. However, the moment when the carrier is acquired and the loop is closed, starting the accumulation, is unknown. This gives rise to an ambiguity term in

the relation between the integrated carrier phase and the current receiver-to-satellite range

$$\phi_{i,k} = \frac{1}{\lambda} \rho_{i,k} + N_i, \quad (8)$$

where λ is the wave-length of the carrier, and N_i is an unknown constant, which for null initial phase accumulation, is $N_i = -\rho_{0,i}/\lambda$. Although N_i can be estimated using ambiguity resolution algorithms, allowing the integrated carrier measurement to be used as a range observable, it can also be time-differenced and so used as a Delta-range measurement [57]. It then becomes a measure of displacement (or average range-rate) rather than of range. This Time-Differenced Carrier Phase (TDCP) pseudo-measurement does not include the influence of N_i , being given by

$$\tilde{\phi}_{k,i} - \tilde{\phi}_{k-1,i} \equiv \Delta\tilde{\phi}_{k,i} = \frac{1}{\lambda} (\Delta\rho_{k,i} + \Delta\rho_{e,k,i}) + \Delta\nu_{\phi,k,i}, \quad (9)$$

where the error term $\Delta\rho_{e,k,i}$ includes contributions from receiver and satellite clocks, atmospheric delays and multipath. $\Delta\nu_{\phi,k,i}$ is measurement noise.

The velocity nature of this pseudo-measurement has led to its use in highly dynamic platforms such as UAV [65] and missile [60]. Its dual-epoch origin, however, makes its use in Kalman filtering more complex than regular measurements. Two possible ways of handling TDCP measurements are:

1. Back-propagation of the up-to-date state and covariance to the previous GNSS epoch as to generate a filter estimate for $\rho_{i,k-1}$ [60].
2. Augmentation of the state vector with a delayed position state (at the previous GNSS epoch), allowing the previous epoch range $\rho_{i,k-1}$ to be given in terms of the current state vector \mathbf{x}_k [57, 65].

While the first method does not involve state augmentation, it requires the computation and storage of the elapsed transition matrix from the previous GNSS epoch to the current, and the evaluation of its inverse, which may be computationally expensive. It also yields a rather complex update model with correlated system and measurement noise and mutually-correlated measurements within the set of channels. The second method, on the other hand, yields a measurement update model of the regular form (no correlations) and can handle sequential measurement processing (or updating) which reduces computational burden. Moreover, as suggested in [57], the augmented position state needs not be updated as it is reset after each measurement update step. It can thus be handled as a *consider* state (cf. Section 6.2), as its value is also constant, partially relieving the burden carried by the augmentation.

5.1.3 Receiver Navigation Solution

A navigation solution is computed by the receiver using several or all of the raw measurements described thus far. Depending on the unit's software, this is

either done through single-epoch methods or filtering algorithms. The position and velocity observable are usually modelled in ECEF frame as

$$\tilde{\mathbf{r}}_{\text{ant}}^E = \mathbf{r}_{\text{ant}}^E + \mathbf{b}_r^E + \boldsymbol{\nu}_r \quad (10)$$

$$\tilde{\mathbf{v}}_{\text{ant}}^E = \mathbf{v}_{\text{ant}}^E + \mathbf{b}_v^E + \boldsymbol{\nu}_v, \quad (11)$$

where \mathbf{b}_r^E and \mathbf{b}_v^E are biases, and $\boldsymbol{\nu}_r$ and $\boldsymbol{\nu}_v$ are noise terms. The underscript *ant* refers to the receiver antenna. As a result of the filtered nature of the receiver solution, the bias and noise in (10)–(11) may be heavily time-correlated. As this time correlation is generally unknown (and potentially variable) it is common to update the hybrid navigation algorithm with it at a lower rate than output by the receiver [21]. This may not be acceptable for highly dynamic applications such as the one at hand.

5.2 Errors and disturbances

The Pseudorange, Pseudorange-rate and Time-differenced Carrier Phase measurement errors in (4), (5) and (9) denoted $\rho_{e,i}$, $\dot{\rho}_{e,i}$ and $\Delta\rho_{e,i}$ may have a variety of origins. These can be expanded as

$$\rho_{e,i} = c\delta t + c\delta t_{\text{sat},i} + \rho_{T,i} + \rho_{I,i} + \rho_{M,i} \quad (12)$$

$$\dot{\rho}_{e,i} = c\dot{\delta t} + c\dot{\delta t}_{\text{sat},i} + \dot{\rho}_{T,i} - \dot{\rho}_{I,i} + \dot{\rho}_{M,i} \quad (13)$$

$$\Delta\rho_{e,i} = c\Delta\delta t + c\Delta\delta t_{\text{sat},i} + \Delta\rho_{T,i} - \Delta\rho_{I,i} + \Delta\rho_{M,i}, \quad (14)$$

where δt and $\dot{\delta t}$ are the receiver clock bias and drift; δt_{sat} is the satellite clock error; terms with T and I are Tropospheric and Ionospheric induced errors; and M denotes multipath effects.

Receiver clock handling is discussed in Section 5.2.1. The Tropospheric and Ionospheric can be (coarsely) corrected as it will be seen in Sections 5.2.2 and 5.2.3. Multi-path may occur due to reflections on vehicle surfaces and can be mitigated by proper antenna placement within the vehicle. The satellite clock offset can be corrected using parameters from the broadcasted navigation message. Any remaining residuals (e.g. due to ephemeris errors) can be accounted for in the filter as bias states.

5.2.1 Receiver clock errors

The receiver clock error affects all channels equally. While the clock bias disturbs range measurements (pseudorange and carrier phase), the clock drift affects the range-rate (Doppler) ones. These clock effects are generally modelled within the navigation filter as a second order system as

$$\begin{bmatrix} \ddot{\tau}_r \\ \dot{\tau}_r \end{bmatrix} = \begin{bmatrix} 0 & 0 \\ 1 & 0 \end{bmatrix} \begin{bmatrix} \dot{\tau}_r \\ \tau_r \end{bmatrix} + \mathbf{w}_{\tau_r}, \quad (15)$$

where the characteristics of the noise $\mathbf{w}_{\tau_r} \sim N(\mathbf{0}, \mathbf{Q}_{\tau_r})$ are obtained, for instance, through Allan variance analysis [10]. This type of stochastic analysis

was used in [57] to approximate the clock frequency noise of a DLR Phoenix-HD receiver as white noise, resulting in a reduced order clock model for a PR and TDCP updated hybrid filter. Note that, depending on the receiver, it may be the case that the common mode error in the pseudorange-rate measurements does not correspond to the drift of the common mode offset of the pseudoranges (or carrier phases). Careful study of the receiver and its outputs should thus precede any modelling.

An alternative to explicitly modelling the clock error is measurement cross-differencing. As implemented in the HNS system flown in the SHEFEX2 mission [52], a pseudo-measurement obtained by subtracting two measurements of the same type is free of the common mode error, and thus of clock bias/drift. This method yields modest computational savings by freeing up two state slots. However, although performance-wise equivalent to explicit modelling, cross-differencing has a drawback: at least two tracked satellites are needed to perform a filter update. Robustness to partial outages is thus potentially reduced. Moreover, cross-differencing couples the noise between different measurements, rendering the measurement covariance matrix non-diagonal. This hinders the use of a sequential measurement updating scheme by requiring measurement pre-whitening [4].

5.2.2 Tropospheric errors

GNSS signals travelling through the Troposphere (up to 50km altitude) suffer refraction. This introduces a transmission delay that depends on signal travel path and atmospheric conditions. On-ground, the experienced delay varies slowly, appearing as position bias. As shown in [57], during launch, in the Tropospheric ascent phase, this delay changes quickly severely affecting the measured GNSS velocity information (range-rate or delta-range). Fig. 8b to 8d display this effect for differenced pseudorange (Delta-PR), pseudorange-rate (PR-rate) and time-differenced Carrier Phases (TDCP), for three different satellite elevations. The trajectory followed is that of SHEFEX2 sounding rocket, whose altitude profile is displayed in Fig. 8a. The signals were measured using a DLR Phoenix-HD GPS receiver stimulated by a GSS7700 SPIRENT GNSS emulator running a NATO STANAG troposphere model [36].

If uncorrected, the hump-like error (especially visible in TDCP) may corrupt the navigation estimation. Fig. 8e to 8g show the same quantities corrected using a simple model, given by [49]

$$\rho_{T,i}(\mathbf{x}) = M(E_i)\Delta(h_a), \quad (16)$$

with

$$M(E_i) = \frac{1.0121}{\sin E_i + 0.0121} \quad (17)$$

$$\Delta(h_a) = 2.4405 e^{-0.133 \times 10^{-3} h_a}, \quad (18)$$

where the *Zenit* delay $\Delta(\cdot)$ is a function of the receiver altitude h_a , and the mapping function $M(\cdot)$ depends on the satellite apparent elevation E_i . Note

that in the case of TDCP (Fig. 8g) the residual after correction is still considerably larger than the channel noise level.

As proposed in [57], the tropospheric correction may be considered to be corrupted by a scale-factor error which is in turn accounted for in the uncertainty filter model for the corrected measurement. Such scale-factor can be treated as noise or estimated as a constant state. Furthermore, it can be defined as a scalar affecting all channels equally or as an array of factors (one per channel). Fig. 9 compares these different correction residual compensation approaches in terms of velocity estimation error of a filter updated with PR and TDCP during lower ascent phase. It is clear that neglecting the leftover residuals renders the filter incoherent. Among the compensated schemes, modelling the correction uncertainty as a single (scalar) scale-factor, rather than a set of factors, yields the greatest improvement. Treating this scalar-factor as noise further decreases the effect on the estimation error. Handling it as measurement noise also has the added advantage of not requiring state augmentation.

5.2.3 Ionospheric errors

The Earth's Ionosphere, between about 50 km and 1000 km of altitude, is a dispersive medium that affects GNSS signal propagation. As the Troposphere, it causes refraction, and thus delay, of the signal modulation (PRN code). However, it advances the carrier phase the same amount; hence the opposite sign of Ionospheric contributions to pseudorange and Doppler or carrier phase measurements (12) and (13)–(14). Dispersive medium means that the propagation velocity varies with signal frequency. This allows the elimination of Ionospheric errors in dual frequency operation (e.g. L1 and L2 in GPS). For single frequency (non-differential) operation correction requires the use models.

As the Tropospheric delay, Ionospheric error is fairly constant for land-based slow-moving receivers. On a launch trajectory, however, it varies quickly with the (relatively) faster changing satellite apparent elevations. Furthermore, as the vehicle climbs the effective Ionospheric thickness above it decreases, further adding to this varying nature. Fig. 10a shows the error induced by the Ionospheric delay-rate on TDCP for a Vega trajectory section starting at 50 km altitude. The measurements were again collected by a DLR Phoenix-HD receiver fed by a GSS7700 SPIRENT GNSS emulator. The altitude profile of the trajectory used is displayed in Fig. 10b, while Fig. 10d shows the apparent elevation history of the tracked satellites. The errors in PR and PR-rate are much lower than the noise levels in these measurements and are thus omitted. Fig. 10a shows that the Ionospheric errors in TDCP are considerably lower than those induced by the Troposphere in the previous section. The error shows an increasing trend with lower elevation and with faster elevation rate.

As mentioned, correction can be done with a delay model. This should account for satellite elevation and changing Ionospheric vertical thickness. Montenbruck et al. [32] propose a model of the form

$$\rho_{1,i} = \frac{40.3}{f^2} M(E_{IP,i}) \text{VTEC}(\mathbf{r}_{IP,i}) , \quad (19)$$

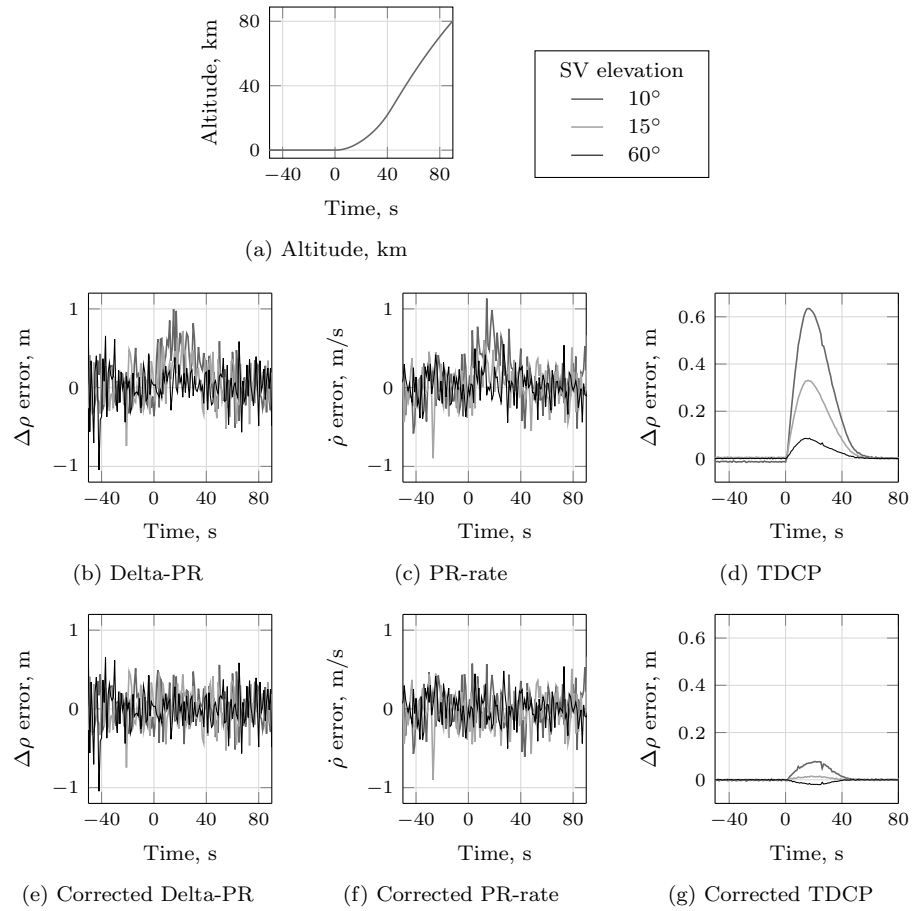


Figure 8: Tropospheric error in Delta-PR, PR-rate and TDCP (at 1Hz) during ascent (lift-off at 0s) before and after model-based correction.

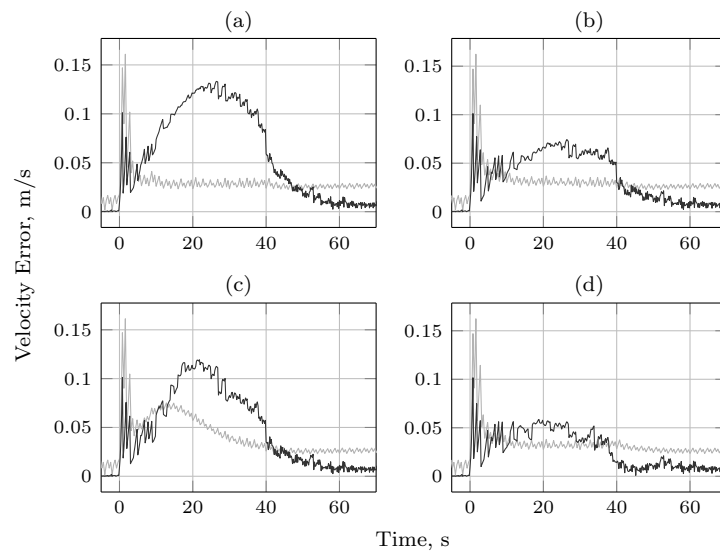


Figure 9: Velocity estimation comparison for different Tropospheric delay correction schemes in a hybrid navigation system with PR and TDCP: a) Tropospheric correction residuals neglected; b) Covariance compensation with single scale-factor error, estimated as state; c) Covariance compensation with one scale-factor error per channel, estimated as states; and d) Covariance compensation with single scale-factor error, treated as noise (no extra state). Trajectory identical to Fig. 8a. Filter $1\text{-}\sigma$ covariance as faded coloured lines.

that accounts for the change of VTEC (Vertical Total Electron Content) with receiver altitude as

$$\text{VTEC}(\mathbf{r}_{\text{IP},i}) = \frac{e - \exp(-z_{\text{IP},i})}{e - \exp(h_0/H)} \text{VTEC}(\mathbf{r}_{\text{IP},i,0}) \quad (20)$$

$$z_{\text{IP}} = \frac{h_{\text{IP},i} - h_0}{H}, \quad (21)$$

where \mathbf{r}_{IP} is the Ionospheric point², the surface (vertical) projection of which is denoted $\mathbf{r}_{\text{IP},i,0}$. f is the L1 frequency, and h_0 and H are, respectively, the inflection point altitude and scale height of the Chapman profile. $M(\cdot)$ is the mapping function accounting for the apparent satellite elevation E_{IP} , in this case with respect to the Ionospheric point. While in [32] $M(\cdot)$ is modelled as a cosecant function, we use the mapping function introduced by Lear [29]

$$M(E) = \frac{2.037}{\sin(E_{\text{IP}}) + \sqrt{\sin^2 E_{\text{IP}} + 0.076}}. \quad (22)$$

The value for the surface VTEC ($\mathbf{r}_{\text{IP},i,0}$) can be computed with a regular Klobuchar model [28] or set to a constant value.

Fig. 10c shows the residuals after correction of the TDCP measurements with the model just described, using a constant surface VTEC of 20 TECU. This time, the residual magnitude is clearly small enough to simply be neglected, however, if deemed necessary, a similar filter robustness scheme to that used in the case of Tropospheric correction could also be used.

5.3 GNSS measurement set and navigation performance

Fig. 11 compares the navigation covariance performance obtained using the following sets of GNSS raw measurements to update the hybrid navigation (EKF) filter under a Vega launcher trajectory:

- GNSS position and velocity (POS+VEL);
- Pseudorange (PR);
- Pseudorange and Pseudorange-rate (PR+PRR); and
- Pseudorange and Time-Differenced Carrier Phase (PR+TDCP).

The inertial sensor is a Tactical-grade FOG-based unit (Table 1) and the GNSS signal performance levels are those of a DLR Phoenix-HD receiver fed by a GSS7700 SPIRENT emulator. (Other receivers with different internal tuning may yield different overall performance.) The results assume Tropospheric and Ionospheric corrections: The raw GNSS measurement models (PR, PRR and

²This is the point, on the line-of-sight from receiver to satellite i , that lies at the altitude of 50 percentile of residual Ionosphere, i.e. the altitude at which half of the VTEC from receiver altitude to infinity is achieved.

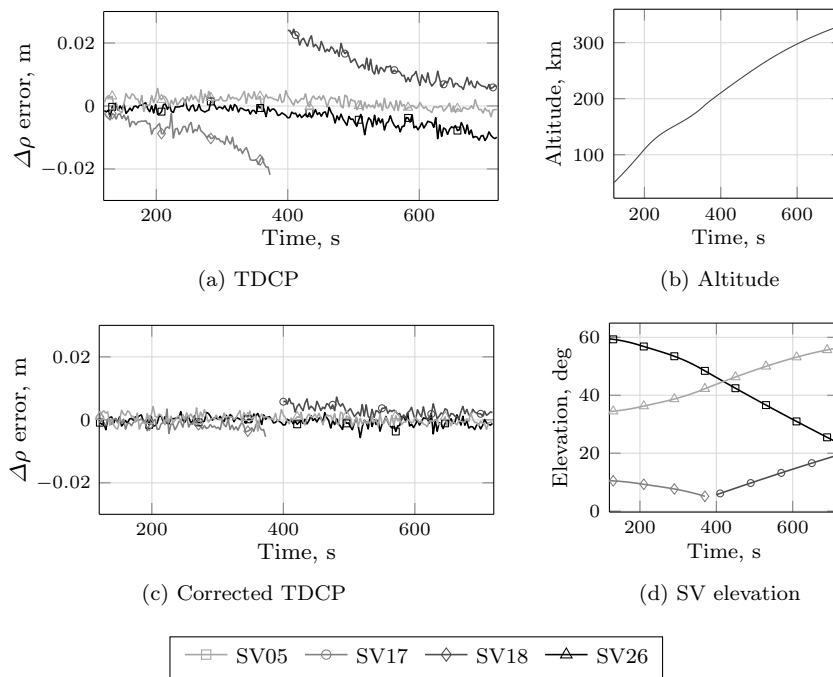


Figure 10: Ionospheric error profile in TDCP (at 1Hz) during ascent (lift-off at 0s) before and after correction.

TDCP) include covariance compensation for the correction uncertainty (cf. Section 5.2.2). The position and velocity measurement models assume these corrections are done at receiver level, thus a (slightly) more conservative tuning is used. This is scheduled by altitude to account for correction residuals.

Comparing the different velocity covariance curves it is clear that the inclusion of velocity-based measurements yields improved estimation of this state. In fact, also attitude is slightly improved with the additional information. Among the raw measurement (tightly coupled) configurations, the one with TDCP clearly provides the most accurate velocity estimates. The PR+PRR set-up presents somewhat marginal improvements over the PR-only configuration. This is explained by the rather high noise level of the Pseudorange-rates retrieved by receiver tested, which has its internal tracking loop tuning set loose enough to minimize loss of lock under high dynamics (hence the initials HD in its name). The performance achieved by the loosely coupled set-up (POS+VEL) approaches that of PR+TDCP because the receiver navigation solution uses Carrier Phase smoothing. The difference which is still visible is due to the conservative tuning of the loosely coupled filter as a defence against atmospheric correction residuals. Expected position accuracy is almost identical among tightly coupled set-ups. The POS+VEL filter shows a slightly different curve as, in this analysis, it did not account for tracked satellite number or geometry in its measurement models. Note that the velocity estimation levels here shown are lower than those in Fig. 6. This is explained by the more conservative tuning of the models used in Fig. 6 which assumed higher uncertainty due to uncorrected atmospheric errors.

In Fig. 12 the main advantage of a tightly coupled as opposed to a loosely coupled configuration is illustrated. Three partial GNSS outages of 30 sec each were introduced in the trajectory data of the previous test. The outages occur in the beginning of each of the three engine burns as if caused by the shocks and vibrations of ignition. In the first, second and third partial outages 1, 2 and 3 satellites are still tracked, respectively. GNSS receiver navigation solution is interrupted in all three occurrences. Fig. 12 presents velocity and attitude covariance history of the PR+TDCP and POS+VEL filters. While for a single remaining satellite the divergence level is fairly similar, in the 2-satellite period the difference is significant. With three satellites the divergence of both states of the tightly coupled configuration is hardly visible. Given the likelihood of signal tracking interruptions during launch, this feature is of great importance in the architecture selection.

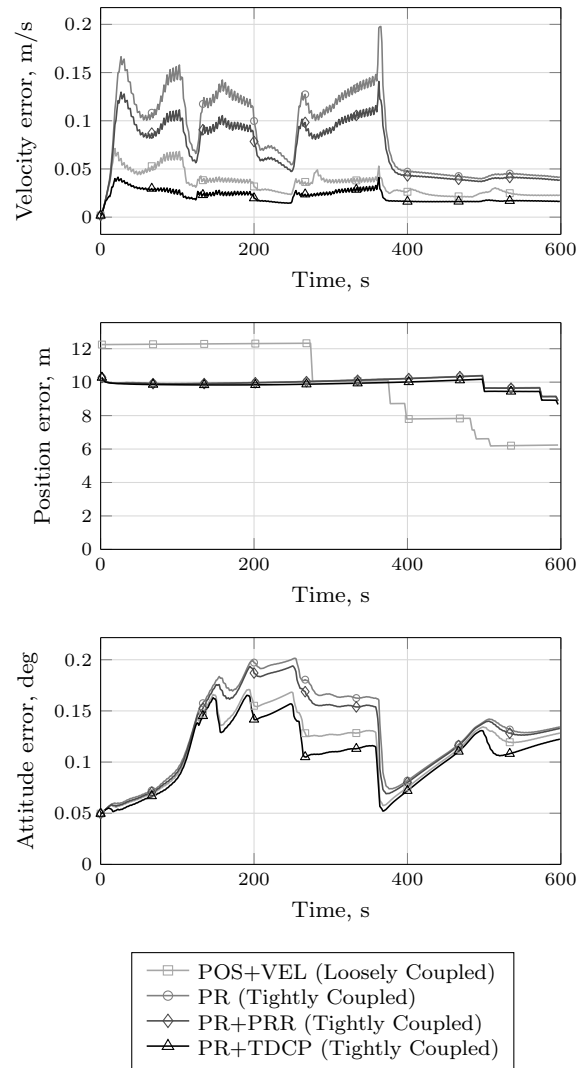


Figure 11: Hybrid navigation performance ($1\text{-}\sigma$ cov.) with different GNSS meas. sets. Vega trajectory.

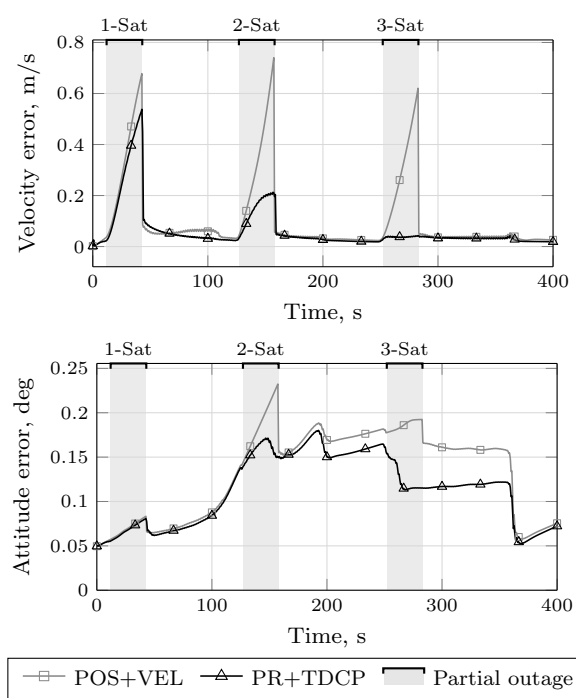


Figure 12: Loose *vs* Tight coupling in GNSS partial outage conditions (1, 2 and 3 satellites tracked).

6 Filter, robustness and fault-tolerance

6.1 Filter algorithm considerations

The propagation and measurement models of a GNSS/INS system may be written

$$\begin{bmatrix} \mathbf{x}_{\text{kin},j+1} \\ \mathbf{x}_{\text{imu},j+1} \\ \mathbf{x}_{\text{gnss},j+1} \end{bmatrix} = \begin{bmatrix} \phi_{\text{kin},j}(\mathbf{x}_{\text{kin},j}, \hat{\mathbf{u}}_{j+1}(\hat{\mathbf{u}}_{j+1}, \mathbf{x}_{\text{imu},j})) \\ \phi_{\text{imu},j}(\mathbf{x}_{\text{imu},j}) \\ \phi_{\text{gnss},j}(\mathbf{x}_{\text{gnss},j}) \end{bmatrix} + \begin{bmatrix} \mathbf{w}_{\text{kin},j} \\ \mathbf{w}_{\text{imu},j} \\ \mathbf{w}_{\text{gnss},j} \end{bmatrix}, \quad (23)$$

and

$$\mathbf{y}_{\text{gnss},j} = \mathbf{h}_{\text{gnss},j}(\mathbf{x}_{\text{kin},j}, \mathbf{x}_{\text{gnss},j}) + \boldsymbol{\nu}_{\text{gnss},j}, \quad (24)$$

where \mathbf{x} are states, \mathbf{w} are process noises and $\boldsymbol{\nu}$ are measurement noises.

The state vector is split into: kinematics states, denoted kin , generally comprising velocity, position and attitude; IMU states, imu , including biases, scale-factors, misalignments, and others; and GNSS measurement model states, gnss , for instance, receiver clock bias/drift and channel/solution biases. The kinematics propagation model, ϕ_{kin} , uses the corrected inertial measurements $\hat{\mathbf{u}}$, computed from the actual measurements $\tilde{\mathbf{u}}$ and the IMU perturbation states \mathbf{x}_{imu} .

A closer look at the structure of the propagation and measurement functions reveals several instances of non-linearities in both of them. The attitude propagation law (in ϕ_{kin}) is non-linear. So are some of the IMU error corrections in $\hat{\mathbf{u}}$, e.g. scale-factors and misalignments (multiplicative perturbations). The measurement mappings of the raw GNSS measurements are either of range or range-rate which are also non-linear. On the other hand, position and velocity measurements (in a loosely coupled design) are given by linear models. Linear is also the propagation of both IMU and GNSS measurement states (functions ϕ_{imu} and ϕ_{gnss}).

The most widely used approach for such a system is the Extended Kalman filter (EKF). This uses the full non-linear model for state integration and innovation computation, and a linearisation of this for covariance propagation and update (Kalman) gain calculation. The non-linear nature of the system has motivated extensive experimentation with more complex non-linear filtering schemes. Wendel et al. [58] observed only marginal performance improvement of the Unscented Kalman filter (UKF), also known as Sigma-Point Kalman filter, in an GPS/INS system with respect to the EKF. (Other authors have reported similar results [20, 40].) The non-linearities in the GNSS raw measurement models and in the kinematics state propagation of both medium and low grade sensors were found to be moderate, and thus well suited for the EKF. Significantly faster convergence by the UKF was however observed for very high errors at initialization. Given the application at hand, this may be of little importance in on-ground initialization (at the launch pad), but rather advantageous in the recovery from long GNSS outages during flight. Note that the computational complexity of the UKF is considerably higher than that of the EKF, making it less attractive in this trade-off.

Another important point to consider in the design of the filter algorithm is the rate of the several steps involved. Assuming a modular (indirect) filtering approach, as defined in Section 3, the fusion algorithm may perform error-state propagation, covariance propagation and measurement update at different rates [50, 57]. The GNSS measurement updates can be performed at the receiver’s output rate (generally 1 Hz) to avoid loss of information. As for the filter prediction steps, as covariance propagation is comparatively more “expensive” than state propagation, this step may be performed at a lower rate than the filter error-state integration. The latter can, in turn, be performed at a (considerably) lower rate than the parallel strapdown propagation. The selection of such propagation rates should be carefully verified under the target vehicle dynamics and trajectory.

6.2 Filter robustness

As seen in previous sections, both IMU and GNSS measurements can be corrupted by numerous error sources. A natural way of making the navigation robust against these is by modelling and estimating their effect within the filtering algorithm. This is not always possible nor practical. From lack of suitable/accurate models, to growth of filter size, there are several drawbacks to this approach. Robustness can still be achieved through other means. Conservative tuning, of which measurement/process-model under-weighting are popular examples, is a common remedy in many cases [64]. The following two instances of this approach were mentioned in previous sections. The SHEFEX2 HNS uses inflated process noise values for inertial sensor scale-factor states to compensate for the unmodeled non-linearities [51]; the HNS also heavily under-weights pseudorange measurements at lower altitudes to render the filter robust against Tropospheric effects [52].

It may be argued that many of the robust (Kalman-like) filter implementations found in literature (e.g. fading memory filters [45]) fall into this set of conservative tuning techniques. Others depart from it by requiring some level of model or uncertainty structure (e.g. \mathcal{H}_∞ Kalman filtering [45]). Within this spectrum, and somewhat closer to full modelling than to simple conservative tuning, lie the Schimdt filtering (or *consider* state filtering) techniques. In this framework, the system and measurement perturbations are modelled as *consider* states, i.e. states for which covariance is modelled but not updated (i.e. explicitly estimated) [8, 63].

In a *consider* Kalman filter design the state vector \mathbf{x} is split into standard states, \mathbf{x}_s , and consider states, \mathbf{x}_c , as

$$\mathbf{x} = \begin{bmatrix} \mathbf{x}_s \\ \mathbf{x}_c \end{bmatrix}. \quad (25)$$

The Kalman gain portion corresponding to the consider states is made null

$$\mathbf{K} = \begin{bmatrix} \mathbf{K}_s \\ \mathbf{K}_c \end{bmatrix} = \begin{bmatrix} \mathbf{K}_s \\ \mathbf{0} \end{bmatrix}, \quad (26)$$

preventing consider state update. In fact, the consider state values and covariances are generally kept completely separate from the main states in the code, effectively yielding a reduced-order filter. Computational load is thus lighter in comparison the full-order filter with all states explicitly estimated.

6.3 Tolerance to faults

Integrity and reliability requirements for launch navigation systems are generally very stringent given the mission- (and even safety-) critical nature of this subsystem. Fault detection is thus a crucial element in the navigation design. As previously mentioned, in “traditional” inertial launcher navigation fault detection and contingency are usually accomplished through redundancy of inertial units (e.g. Ariane-V). The inclusion of GNSS measurements adds an important source of redundant information.

Most GNSS receivers use RAIM (Receiver Autonomous Integrity Monitoring) routines to verify the sanity of their measurements. These are based on self-consistency tests generally performed through snapshot (single-epoch) methods such as Solution Separation or Least-squares Residuals [6].

In hybrid GNSS/INS systems, the (*a-priori*) filter innovations can be used to test the sanity of each new set of GNSS measurements. Rather than a self-consistency test, this method compares the new GNSS information with the inertially propagated previous GNSS history, effectively increasing GNSS failure detection levels. Testing single innovations also allows the identification and rejection of single-channel outliers [39]. This can be done through sequential processing with or without covariance decoupling of the measurements.

A combination of RAIM-like self-consistency algorithms with filter innovation testing may go a step further and allow identification of not only single- (or multiple-) channel outliers, but also common-mode (receiver clock) faults and inertial propagation faults. Note that both receiver clock faults and excessive inertial propagation divergence (during GNSS latency or outage) will result in generalized innovation failure (violation of some pre-defined threshold). By parallelly checking the self-consistency of the GNSS measurement set, the system is able to tell these faults apart from multiple channel failure (e.g. severe Ionospheric perturbations or multipath effects). In case of consistent measurement set, distinction between common-mode receiver fault and excessive inertial divergence can then be done through the comparison of GNSS-only position/clock solution and the corresponding filter state values. Filter recovery is done by covariance inflation of the affected states (position/velocity or clock bias/drift) followed by regular measurement update. This proposed Fault Detection, Isolation and Recovery (FDIR) scheme is depicted in Fig. 13.

7 Conclusion

In this work we investigated several of the key architectural elements and design aspects of hybrid GNSS/INS navigation when applied to space transportation.

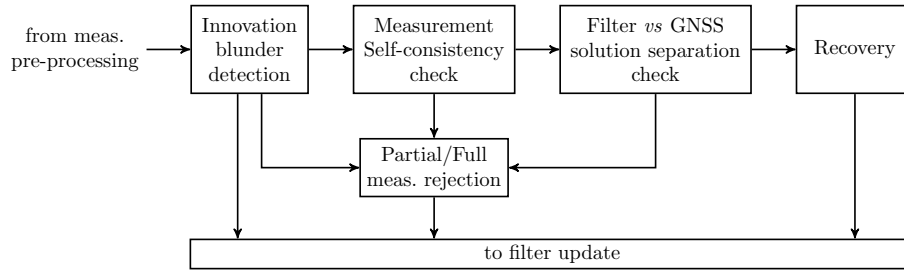


Figure 13: Proposed FDIR scheme for hybrid navigation combining innovation testing and RAIM-like GNSS self-consistency checking.

The numerous limitations of the pure-inertial navigation way has raised wide interest in the use of GNSS-based technologies in this area. A broad range of GNSS application examples and studies were presented together with a collection of possible requirements and challenges for the design of launcher hybrid navigation systems.

Several coupling depths of hybrid navigation were looked into. Among these, the Tightly coupled way offers a high flexibility and robustness options, being realizable with COTS components. Deeper in the design, a closed-loop scheme, with inertial propagation corrected by the system estimates, prevents unbounded filter state growth and allows online inertial calibration, effectively improving robustness and performance during free propagation. A modular design, with separate strapdown and fusion algorithm routines, allows parallelization and means of coping with GNSS output latency.

In what concerns the inertial part of the system, propagation algorithm and rate are crucial elements in a highly dynamic application. Integration rate reduction can be achieved using compensation algorithms; however, only mild reductions (2-3 times) seem possible in the application at hand. Use of lower grade inertial sensors may require additional states in the fusion algorithm to account for higher than first-order bias models, axis misalignments, and bias/scale-factor g-dependencies. Covariance analysis showed that the fusion of GNSS fixes with INS data not only restricts the errors in these states to GNSS levels, but also grants some attitude observability. This yielded an attitude estimation improvement in a Vega scenario of about one grade with respect to the inertial-only set-up.

Among the GNSS outputs, Position, Velocity, Pseudorange, Pseudorange-rate, Carrier Phase measurements were considered. From the latter measurement a time-differenced pseudo-measurement can be created (Time-Differenced Carrier Phases - TDCP) which is a measure of displacement and is free from phase ambiguity. Modelling of the clock offset in all raw GNSS measurements is preferable to measurement cross-differencing as it allows sets down to a single satellite to be used. Atmospheric effects on velocity-based GNSS measurements were found to be considerably amplified by the vehicle's speed, through climb rate and increased apparent elevation-rate of tracked satellites. Atmospheric

corrections, even with coarse models, greatly improve velocity estimation; however, correction residuals, especially of Tropospheric delay, need to be accounted for in the measurement model. Covariance analysis of hybrid set-ups with different sets of the GNSS measurements (in a Vega scenario) showed the importance of velocity-based measurements as support to position-based ones. It also emphasised the superior velocity estimation achieved with the TDCP measurement. The Tightly coupled set-up with PR and TDCP showed far less divergence than the loosely coupled equivalent (POS+VEL) under partial GNSS outages of fewer than four satellites.

Finally turning to the filter core, given the moderate non-linearities in the strapdown propagation equations and in the range and range-rate models, more complex algorithms than the EKF are generally unnecessary. In terms of filter robustness, the Consider state filter design allows error contributions to be modeled and accounted for without explicitly estimating them within the filter. This yields a reduced-order filter with robustness against structured uncertainties. Fault tolerance, a major requirement of any launcher navigation system, can be accomplished through an FDIR scheme combining innovation and measurement self-consistency tests. Such a scheme allows for detection and isolation of faults in both GNSS single/multiple channels and strapdown propagation.

Acknowledgements

The authors would like to thank ESA, Guidance, Navigation & Control Section at the European Space Research and Technology Centre for granting the funding, through the Network/Partnering Initiative contract 4000111837/14/NL/MH, which enabled this research. In addition, the authors would like to thank Samir Bennani from the Guidance, Navigation & Control Section at ESA, and Oliver Montenbruck, Markus Markgraf and Benjamin Braun from the German Space Operations Center of DLR for the support to this work.

References

- [1] *Atlas V Launch Services User's Guide*. United Launch Alliance. U.S., Mar. 2010.
- [2] N. M. Barbour. "Inertial Navigation Sensors." In: *Advances in Navigation Sensors and Integration Technology*. NATO RTO Lecture Series-232. NATO, 2003.
- [3] S. Belin, S. Villers, and A. Conde Reis. "Requirements toward GNSS chain for Ariane 5 Mid-Life Evolution." In: *5th ESA Workshop on Satellite Navigation Technologies and European Workshop on GNSS Signals and Signal Processing (NAVITEC)*. 2010. DOI: 10.1109/NAVITEC.2010.5708078.
- [4] G. J. Bierman. *Factorization Methods for Discrete Sequential Estimation*. Ed. by R. Bellman. Academic Press, 1977.
- [5] B. Braun, M. Markgraf, and O. Montenbruck. "Performance analysis of IMU-augmented GNSS tracking systems for space launch vehicles." In: *CEAS Space Journal* 8.2 (2016), pp. 117–133. DOI: 10.1007/s12567-016-0113-9.

- [6] R. G. Brown. "Global Positioning System: Theory and Applications." In: ed. by B. W. Parkinson and J. J. Spilker Jr. Vol. 2. AIAA, 1996. Chap. Receiver Autonomous Integrity Monitoring.
- [7] E. Burke, E. Rutkowski, and E. Rutkowski. "Vehicle Based Independent Tracking System (VBITS): A Small, Modular, Avionics Suite for Responsive Launch Vehicle and Satellite Applications." In: *6th Responsive Space Conference*. 2008.
- [8] J. L. Crassidis and J. L. Junkins. *Optimal Estimation of Dynamic Systems*. Chapman & Hall/CRC, 2012.
- [9] *Delta IV Launch Services User's Guide*. United Launch Alliance. U.S., June 2013.
- [10] A. J. van Dierendonck, J. B. McGraw, and R. G. Brown. "Relationship Between Allan Variances and Kalman Filter Parameters." In: *16th Annual PTTI Meeting*. 1984.
- [11] V. D. Dishel and E. L. Mezheritskiy. "Principals Of Integrated INS/GLONASS+GPS GNC Systems For Space Launchers. Results Of Realized Missions And Future Prospects." In: *8th International ESA Conference on Guidance, Navigation & Control Systems*. June 2011.
- [12] S. Dussy, D. Durrant, T. Moy, N. Perriault, and B. Celerier. "MEMS gyro for space applications: Overview of European activities." In: *AIAA Guidance, Navigation and Control Conference and Exhibit*. 2005. DOI: 10.2514/6.2005-6466.
- [13] B. Ferrell, J. Simpson, R. Zoerner, J. B. Bull, and R. J. Lanzi. "Autonomous Flight Safety System." In: *41st Space Congress*. 2004.
- [14] M. Giannini, M. Melara, and C. Roux. "ALTS Localization System Of Vega Launcher: VV02 Post-Flight Analysis & GPS Issues For Future Hybrid Navigation." In: *9th International ESA Conference on Guidance, Navigation & Control Systems*. June 2014.
- [15] *Global Positioning and Inertial Measurements Range Safety Tracking Systems' Commonality Standard*. RCC 324-01. Range Commanders Council, 2001.
- [16] S. Gomez. *Three Years of Global Positioning System Experience on International Space Station*. NASA/TP-2006-213168. NASA. Houston, Texas, U.S., Aug. 2006.
- [17] S. Gomez and M. Lammer. "Lessons Learned from Two Years of On-Orbit Global Positioning System Experience on International Space Station." In: *ION-GNSS Meeting*. Long Beach, U.S., 2004.
- [18] S. Gonseth, F. Rudolf, C. Eichenberger, D. Durrant, and P. Airey. "Miniaturized high-performance MEMS accelerometer detector." In: *CEAS Space Journal 7.2* (2015), pp. 263–270. DOI: 10.1007/s12567-015-0093-1.
- [19] M. S. Grewal, L. R. Weill, and A. P. Andrews. *Global Positioning Systems, Inertial Navigation, and Integration*. Wiley & Sons, 2001.
- [20] J. Gross, Y. Gu, S. Gururajan, B. Seanor, and M. R. Napolitano. "A Comparison of Extended Kalman Filter, Sigma-Point Kalman Filter, and Particle Filter in GPS/INS Sensor Fusion." In: *AIAA Guidance, Navigation, and Control Conference*. 2010. DOI: 10.2514/6.2010-8332.

- [21] P. D. Groves. *Principles of GNSS, Inertial, and Multisensor Integrated Navigation Systems*. Artech House, 2008.
- [22] X. Guochang. *GPS Theory, Algorithms and Applications*. 2nd Ed. Springer, 2007.
- [23] A. Hauschild, M. Markgraf, O. Montenbruck, H. Pfeuffer, E. Dawidowicz, B. Rmili, and A. Conde Reis. “Results of the GNSS Receiver Experiment OCAM-G on Ariane-5 flight VA 219.” In: *6th European Conference for Aeronautics and Space Sciences (EUCASS)*. Krakow, Poland, June 2015.
- [24] H. Hou. “Modeling Inertial Sensors Errors Using Allan Variance.” PhD thesis. University of Calgary, 2004.
- [25] M.B. Ignagni. “Efficient Class of Optimized Coning Compensation Algorithms.” In: *Journal of Guidance, Control and Dynamics* 19.2 (1996), pp. 424–429. DOI: 10.2514/3.21635.
- [26] *Independent Assessment of X-37 Safety & Mission Assurance Processes and Design Features*. NASA Headquarters Office of Safety & Mission Assurance. U.S., June 2001.
- [27] E. D. Kaplan and C. J. Hegarty. *Understanding GPS: Principles and Applications*. 2nd. Artech House, 2006.
- [28] J.A. Klobuchar. “Global Positioning System: Theory and Applications.” In: ed. by B. W. Parkinson and J. J. Spilker Jr. AIAA, 1996. Chap. Ionospheric effects on GPS.
- [29] W.M. Lear. *GPS navigation for low-earth orbiting vehicles*. NASA 87-FM-2, JSC-32031. Rev. 1. NASA, Lyndon B. Johnson Space Center, 1987.
- [30] M. Markgraf and O. Montenbruck. “Phoenix-HD - A Miniature GPS Tracking System for Scientific and Commercial Rocket Launches.” In: *6th International Symposium on Launcher Technologies*. 2005.
- [31] R. A. McKern. “A Study of Transformation Algorithms for Use in a Digital Computer.” MA thesis. University of Illinois, 1968.
- [32] O. Montenbruck and E. Gill. “Ionospheric Correction for GPS Tracking of LEO Satellites.” In: *The Journal of Navigation* 55.2 (2002), pp. 293–304. DOI: 10.1017/S0373463302001789.
- [33] O. Montenbruck and M. Markgraf. “Global Positioning System Sensor with Instantaneous-Impact-Point Prediction for Sounding Rockets.” In: *Journal of Spacecraft and Rockets* 41.4 (2004), pp. 644–650. DOI: 10.2514/1.1962.
- [34] Narmada, S. Reynaud, P. Delaux, and A. Biard. “Use of GNSS for Next European Launcher Generation.” In: *6th International ESA Conference on Guidance, Navigation & Control Systems*. Loutraki, Greece, Oct. 2005.
- [35] S. Nassar. “Improving the Inertial Navigation System (INS) Error Model for INS and INS/DGPS Applications.” PhD thesis. University of Calgary, 2003.
- [36] *NATO Standardization Agreement (STANAG)*. Doc. 4294, Edition 1. NATO, 1993.
- [37] *Orion: America’s Next Generation Spacecraft*. NP-2010-10-025-JSC. NASA, Johnson Space Center. Houston, Texas, U.S., 2010.

- [38] B. W. Parkinson and J. J. Spilker Jr. *Global Positioning System: Theory and Applications*. Vol. 2. AIAA, 1996.
- [39] M. G. Petovello. “Real-Time Integration of a Tactical-Grade IMU and GPS for High-Accuracy Positioning and Navigation.” PhD thesis. University of Calgary, 2003.
- [40] M. St-Pierre and D. Gingras. “Comparison between the unscented Kalman filter and the extended Kalman filter for the position estimation module of an integrated navigation information system.” In: *IEEE Intelligent Vehicle Symposium*. 2004. DOI: 10.1109/IVS.2004.1336492.
- [41] B. Polle, B. Frapard, S. Reynaud, S. Belin, P.A. Krauss, F. Zangerl, L.F. Peñin, V. Fernandez, P. D’Angelo, R. Draï, and T. Voirin. “Robust INS/GPS Hybrid Navigator Demonstrator Design for Launch, Re-entry and Orbital Vehicles.” In: *7th International ESA Conference on Guidance, Navigation & Control Systems*. Ireland, 2008.
- [42] P. G. Savage. “Strapdown Inertial Navigation Integration Algorithm Design Part 1: Attitude Algorithms.” In: *Journal of Guidance, Control and Dynamics* 21.1 (1998), pp. 19–28. DOI: 10.2514/2.4228.
- [43] P. G. Savage. “Strapdown Inertial Navigation Integration Algorithm Design Part 2: Velocity and Position Algorithms.” In: *Journal of Guidance, Control and Dynamics* 21.2 (1998), pp. 208–221. DOI: 10.2514/2.4242.
- [44] M. Schlotterer. “Navigation System for Reusable Launch Vehicle.” In: *31st Annual AAS Guidance and Control Conference*. 2008.
- [45] D. Simon. *Optimal State Estimation*. Wiley & Sons, 2006.
- [46] J. Simpson, C. Campbell, R. Carpenter, E. Davis, S. Kizhner, E. G. Lightsey, G. Davis, and L. Jackson. “Testing of the International Space Station and X-38 Crew Return Vehicle GPS Receiver.” In: *12th International Technical Meeting of the Satellite Division of The ION*. 1999.
- [47] S. Slivinsky, C. Nesbit, C. Bartone, R. Phillips, and R. Rexrode. “Development and Demonstration of a Ballistic Missile Range Safety Technology System.” In: *Journal of the Institute of Navigation* 49.2 (2002), pp. 91–102. DOI: 10.1002/j.2161-4296.2002.tb00258.x.
- [48] P. D. Solomon, J. Wang, and C. Rizos. “Latency Determination and Compensation in Real-Time GNSS/INS Integrated Navigation Systems.” In: *International Archives of the Photogrammetry, Remote Sensing and Spatial Information Science* 38.1 (2011).
- [49] J. J. Spilker Jr. “Global Positioning System: Theory and Applications.” In: ed. by B. W. Parkinson and J. J. Spilker Jr. Vol. 1. AIAA, 1996. Chap. Tropospheric Effects on GPS.
- [50] S. R. Steffes. “Computationally Distributed Real-Time Dual Rate Kalman Filter.” In: *Journal of Guidance, Control and Dynamics* 37.4 (2014), pp. 1064–1068. DOI: 10.2514/1.G000179.
- [51] S. R. Steffes. “Development and Analysis of SHEFEX-2 Hybrid Navigation System Experiment.” PhD thesis. University of Bremen, Apr. 2013.
- [52] S. R. Steffes. “Real-Time Navigation Algorithm for the SHEFEX2 Hybrid Navigation System Experiment.” In: *AIAA Guidance, Navigation, and Control Conference*. 2012. DOI: 10.2514/6.2012-4990. URL: <http://elib.dlr.de/79772/>.

- [53] S. R. Steffes, S. Theil, and M. A. Samaan. "Post-Mission Analysis Of Flight Results From The SHEFEX2 Hybrid Navigation System." In: *9th International ESA Conference on Guidance, Navigation & Control Systems*. Porto, Portugal, June 2014.
- [54] Y. Tang, W. Zhong, J. Shou, and W. Hu. "Exploration of BD2/SINS Deeply Integrated Navigation in CZ-7 Launch Vehicle Guidance System." In: *China Satellite Navigation Conference (CSNC)*. Vol. 3. 2014.
- [55] S. Theil, S. R. Steffes, M. A. Samaan, and M. Conradt. "Hybrid Navigation System for Spaceplanes, Launch and Re-Entry Vehicles." In: *16th AIAA/DLR/DGLR International Space Planes and Hypersonic Systems and Technologies Conference*. 2009.
- [56] D. Titterton and J. Weston. *Strapdown Inertial Navigation Technology*. 2nd Ed. The Institution of Electrical Engineers, 2004.
- [57] G. F. Trigo and S. Theil. "Improved Hybrid Navigation for Space Transportation." In: *4th CEAS Specialist Conference on Guidance, Navigation & Control*. Warsaw, Poland, 2017.
- [58] J. Wendel, J. Metzger, R. Moenikes, A. Maier, and G. F. Trommer. "A Performance Comparison of Tightly Coupled GPS/INS Navigation Systems based on Extended and Sigma Point Kalman Filters." In: *Journal of the Institute of Navigation* 53.1 (2006), pp. 21–32. DOI: 10.1002/j.2161-4296.2006.tb00368.x.
- [59] J. Wendel, C. Schaile, and G. F. Trommer. "Direct Kalman Filtering of GPS/INS for Aerospace Applications." In: *International Symposium on Kinematic Systems in Geodesy, Geomatics and Navigation*. 2001.
- [60] J. Wendel and G. F. Trommer. "Tightly coupled GPS/INS integration for missile applications." In: *Aerospace Science and Technology* 8.7 (2004), pp. 627–634. DOI: 10.1016/j.ast.2004.07.003.
- [61] A. Williams, M. Villa, and J. Puig-Suari. "Platform Independent Launch Vehicle Avionics." In: *28th Annual AIAA/USU Conference on Small Satellites*. 2014.
- [62] B. Willms. "Space Integrated GPS/INS (SIGI) Navigation System for the Space Shuttle." In: *18th Digital Avionics Systems Conference*. 1999.
- [63] D. P. Woodbury. "Accounting for Parameter Uncertainty in Reduced-Order Static and Dynamic Systems." PhD thesis. Texas A&M University, 2011.
- [64] R. Zanetti, K. J. DeMars, and R. H. Bishop. "Underweighting Nonlinear Measurements." In: *Journal of Guidance, Control and Dynamics* 33.5 (2010). DOI: 10.2514/1.50596.
- [65] J. Zhou, S. Knedlik, and O. Loffeld. "Sequential Processing of Integrated Measurements in Tightly-coupled INS/GPS Integrated Navigation System." In: *AIAA Guidance, Navigation, and Control Conference*. 2010. DOI: 10.2514/6.2010-8190.